J Mol Model (2009) 15:581–590
DOI 10.1007/s00894-008-0436-3

ORIGINAL PAPER

Linear and nonlinear optical properties of azobenzene derivatives

P. Krawczyk · A. Kaczmarek · R. Zaleśny · K. Matczyszyn · W. Bartkowiak · M. Ziółkowski · P. Cysewski

Received: 3 October 2008 / Accepted: 25 November 2008 / Published online: 14 January 2009

Abstract The results of computations of spectroscopic parameters of lowest–lying electronic excited states of azobenezene derivatives are presented. The analysis of experimentally recorded spectra was supported by quantum chemical calculations using density functional theory. The theoretically determined resonant (two-photon absorption probabilities) and non-resonant (first-order hyperpolarisability) nonlinear optical properties are also discussed, with an eye towards the performance of recently proposed long-range corrected (LRC) schemes (LC–BLYP and CAM–B3LYP functionals).

Electronic supplementary material The online version of this article (doi:10.1007/s00894-008-0436-3) contains supplementary material, which is available to authorized users.

P. Krawczyk · P. Cysewski
Department of Physical Chemistry, Collegium Medicum,
Nicolaus Copernicus University,
Kurpińskiego 5,
85-950 Bydgoszcz, Poland

A. Kaczmarek (✉)
Faculty of Chemistry, Nicolaus Copernicus University,
Gagarina 7,
87 100 Toruń, Poland
e-mail: teoadk@chem.uni.torun.pl

R. Zaleśny · K. Matczyszyn · W. Bartkowiak
Institute of Physical and Theoretical Chemistry,
Wroclaw University of Technology,
Wybrzeże Wyspiańskiego 27,
50-370 Wrocław, Poland

M. Ziółkowski
Department of Chemistry,
The Lundbeck Foundation Centre for Theoretical Chemistry,
University of Aarhus,
Langelandsgade 140,
8000 Åarhus C, Denmark

Keywords Photoswitching · Density functional theory · CAM-B3LYP functional · Azobenzenes · Electronic excited states · Charge-transfer excitations

Introduction

The molecule azobenzene and its derivatives have attracted the interest of numerous research groups in recent decades [1–13]. Due to their peculiar photoswitching properties, these molecules are used in many areas of molecular electronics [8–10]. Therefore, the mechanism of cis–trans isomerisation, as well as the electronic properties, of azobenzene derivatives remain extensively studied [2, 3, 5, 7]. It is well known that electrowithdrawing and electrodonating substituents can strongly affect the electronic spectra of azobenzene dyes, i.e. $\pi \rightarrow \pi^*$ excitation energies. The stronger the influence of the substituent, the larger the reorganisation of electronic density that can occur upon photoexcitation. This, however, imposes some restrictions with respect to the computational techniques used for theoretical analysis of electronic excitation in azobenzene derivatives. The relatively large size of the systems of interest places most ab initio techniques outside the area of applicability. The configuration interaction with single excitation (CIS) method as well as time-dependent density functional theory (TDDFT) seem to be the two most popular approaches to calculating excitation spectra [14–22]. While the former usually provides values of excitation energies that are too large, the latter is known to suffer from incorrect description of charge–transfer and Rydberg states. An application of exchange-correlation functionals based on local density approximation (LDA), generalised gradient approximation (GGA) or even meta-GGA within the DFT may still lead to improper description of long-range charge distribution modifications [22].

In order to alleviate the above-mentioned issues, a Coulomb-attenuated DFT (CAM–B3LYP), applying the long-range correction recommended by Tsuneda et al. has been proposed recently [23–25]. In a previous study, we have shown that both B3LYP and PBE0 functionals provide excitation energies close to experimental values for a series of trans-azobenzene derivatives [1]. The goal of the present work was to support experimental data with an analysis of the nature of the photoexcitation, with an eye towards assessment of the reliability of predictions of electronic spectra for cis-azobenzene derivatives calculated using the frequently applied conventional global hybrid PBE0 and B3LYP functionals, as well as the recently developed range-separated CAM–B3LYP and LC–BLYP functionals. In addition to linear electro-optic properties, nonlinear optical properties will also be considered. In particular, we will pay attention to the performance of long-range corrected schemes with regards to predictions of molecular (hyper)polarisability for both cis- and trans-azobenzene derivatives. However, the main purpose of this work remains the analysis of how linear and nonlinear optical properties are affected upon modification of the azobenzene core unit. The selected substituents exhibit different donor–acceptor character.

Experimental methods

The series of three polymethylmethacrylate (PMMA) derivatives was synthesised by P. Raimond (Commissariat à l'Energie Atomique, Saclay, France). The azobenzene side chains were attached to 35% (mm) of the PMMA units. The investigated copolymers were dissolved in 1,1,2–trichloroethane (spectroscopic grade, molar concentration 10^{-4} M; Merck, Darmstadt, Germany). The UV–VIS spectra were measured with a Perkin-Elmer Lambda 20 spectrophotometer equipped with a Peltier thermostat and an external source of light. Samples were irradiated with a mercury lamp (200 W Hg, high pressure) and a combination of appropriate interference filters (UV power $I_0=1.15\times10^{-3}$ W/m^2, VIS power $I_0=7.0\times10^{-6}$ W/m^2). The cis-form of the studied materials was achieved after irradiation with UV light of the appropriate wavelength.

Computational methodology

Since, upon irradiation, the excitation in the investigated copolymers occurs in the side chain, all the calculations were performed for azobenzene derivatives mimicking the PMMA copolymers (see Fig. 1). In a recent paper we have shown that such a choice of model system was reasonable and gave quantitively correct results [1].

To properly characterise the excitation energies of the investigated systems, it was essential to choose the level of theory appropriately. The size of the azobenzene derivatives studied in the present contribution suggests that DFT methods be chosen. Careful investigation of the necessary basis set size and the performance of various functionals was carried out on the example of molecule cis–**I** in vacuo to confirm the reliability of the chosen methodology. The RI–CC2 technique [26] as implemented in Turbomole V5.9.1 package [27] was also employed. The basis sets used in these calculations were 6–311++G(d,p) and auxiliary QZVPP [28].

The majority of the results presented in this contribution was obtained with the Gaussian 03 suite of programs [29]. The geometry optimisation for all the investigated molecules (**I**–**III**) was carried out at the B3LYP/6–311++G(d,p) level of theory, both in vacuo and with the inclusion of solvent effects using the value of a dielectric constant corresponding to that of 1,1,2–trichloroethane. Integral equation formalism for the polarisable continuum model (IEF–PCM) was applied to include solvent effects [30]. By means of harmonic vibrational analysis, all structures were confirmed to correspond to the minima on the potential energy surface. In order to investigate the influence of the structure of the analysed systems on UV–VIS spectra, geometry optimisation of cis–**I** in vacuo was also carried out at the MP2/6–311++G(d,p) level of theory.

The wavelengths corresponding to transitions to the lowest–lying excited states, λ_{max}, and oscillator strengths, f, for all three investigated cis–azobenzene derivatives were obtained at the TDDFT/6–311++G(d,p) level. The standard

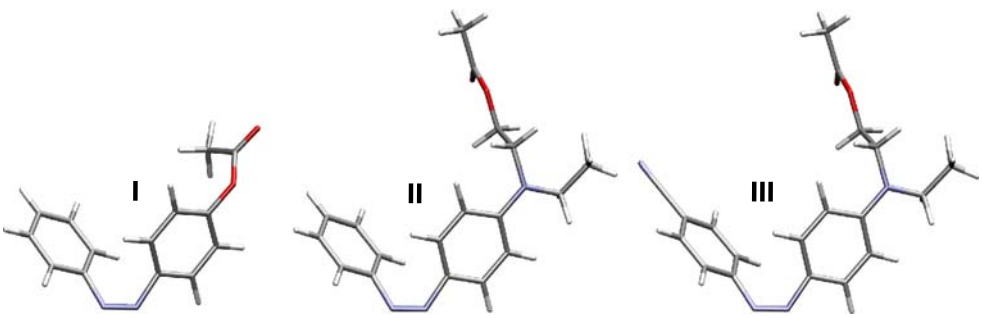

Fig. 1 Structures of the investigated molecules. ***I*** Ph-N=N-Ph-OC(O)CH33, ***II*** Ph-N=N-Ph-N$(C_2H_5)(CH_2)_2OC(O)CH_3$, ***III*** NC-Ph-N=N-Ph-N(C_2H_5) $(CH_2)_2OC(O)CH_3$

hybrid functionals B3LYP and PBE0 were employed in calculations. The solvent effects were likewise considered by means of IEF–PCM.

Since both hybrid functionals used in this study are known to suffer from improper long–range description—which can be critical, particularly for systems with electronic excited states of significantly different polarity to that of the ground state—spectral calculations were additionally repeated in vacuo with the use of CAM–B3LYP [23–25, 31] and LC–BLYP [32, 33] functionals. The dipole moments of excited states were determined by numerical differentiation of excited state energies with respect to electric field strength [34].

The B3LYP/6-311++G(d,p) optimised geometries were used as the starting point for two-photon absorption (TPA) and non-resonant nonlinear optical properties (NLO) calculations. TPA probabilities were computed by applying the response functions at the HF and DFT (B3LYP, PBE0 and CAM–B3LYP) levels of theory, and, for (hyper)polarisabilities, the MP2 and HF methods were employed in addition to BLYP and LC–BLYP DFT functionals. The long-range corrected functionals are expected to provide significant improvement over the conventional pure and hybrid functionals in the NLO properties estimation [25, 33]. All these calculations were performed with the 6-31+G(d) basis set, as recommended by Suponitsky et al. [35] as reproducing well the hyper-polarisability ratios for large organic push–pull molecules. It should also be noted that, while TPA and non-resonant NLO calculations are presented for both cis and trans forms of the investigated compounds, the one-electron absorption section for cis-conformers is discussed here as a supplementary part of a former contribution that presented detailed electron spectra analysis for trans-azobenzene derivatives [1].

Results and discussion

One-photon absorption spectra

The results of calculations of gas phase spectroscopic parameters obtained for four different functionals, namely PBE0, B3LYP, CAM–B3LYP and LC–BLYP, are presented in Table 1. Two important features of gas phase excitation spectra are worth highlighting. Firstly, the increase in the calculated wavelength for the $\pi \rightarrow \pi^*$ transition while proceeding along the series of the systems with growing donor–acceptor strength of substituents (from cis–**I** to cis–**III**) should be noted. Going from cis–**I** to cis–**II**, one observes enhancement of the λ_{max} for the 3^1A state by 45 nm, 44 nm, 37 nm and 34 nm, respectively, for B3LYP, PBE0, CAM–B3LYP and LC–BLYP functionals. Likewise, going from cis–**II** to cis–**III**, the corresponding wavelengths are raised further by 19 nm, 18 nm, 11 nm and 11 nm, respectively, for the above mentioned functionals. It should be stressed that wavelength differences for the various systems are similar for B3LYP and PBE0 functionals, while the CAM–B3LYP data deviate from them substantially.

Secondly, comparison of the wavelengths corresponding to excitation from the ground state to the 3^1A state of all the systems studied obtained for different functionals allows to judge the applicability of the approach adopted in this study to the further analysis of azobenzene derivatives. This is an important point, since it has been proven recently that, even considering only the family of organic dyes, the quality of the TDDFT results obtained can be highly system-dependent and data published to date do not allow generalisation of the conclusions to the universal case. The PBE0 functional has been shown to give very accurate excitation energies for various types of dye molecules provided the extended basis set is used in

Table 1 311++G(d,p) level of theory. Excitation energies calculated for MP2/6–311++G(d,p) optimised geometry are given in parentheses

	B3LYP		PBE0		CAM–B3LYP		LC–BLYP	
	λ_{max}	f	λ_{max}	F	λ_{max}	F	λ_{max}	f
cis–**I**								
2^1A	485 (453)	0.04	478 (445)	0.04	464	0.03	472	0.02
3^1A	305 (316)	0.09	294 (305)	0.12	268	0.20	259	0.21
4^1A	298 (305)	0.02	287 (294)	0.03	261	0.03	253	0.05
cis–**II**								
2^1A	493	0.08	485	0.07	467	0.06	476	0.04
3^1A	350	0.27	338	0.31	305	0.42	293	0.47
4^1A	312	0.03	301	0.03	276	0.04	273	0.04
cis–**III**								
2^1A	501	0.10	492	0.10	465	0.07	479	0.06
3^1A	369	0.27	356	0.31	316	0.47	304	0.53
4^1A	316	0.02	303	0.02	277	0.07	273	0.04

calculations [36–38]. On the other hand, the widely used B3LYP functional is known to slightly overestimate the corresponding wavelengths for dyes [39]. Subsequently, CAM–B3LYP and LC–BLYP were proposed as a remedy for shortcomings of conventional hybrid functionals, and have proved more suitable for the description of long–range phenomena [23–25]. In the particular case of azobenzene dyes, as well as for some other groups of organic dyes, global hybrid functionals seem to outperform range-separated hybrid functionals in terms of the mean average error; however, long-range corrected functionals have been shown to better mimic auxochromic shifts. Nevertheless, large discrepancies still appear in the available surveys and simultaneously surprising results are constantly reported in this field [36, 37].

In the present study, the calculated wavelengths for the $\pi \rightarrow \pi^*$ transition in all the analysed systems construct the following sequence:

$$\lambda_{max}(\mathrm{LC-BLYP}) < \lambda_{max}(\mathrm{CAM-B3LYP}) < \lambda_{max}(\mathrm{PBE0}) < \lambda_{max}(\mathrm{B3LYP}).$$

This trend is consistent with the amount of exact exchange included in the applied functionals (B3LYP containing 20% of the HF exchange; PBE0 –25% and CAM–B3LYP varying from 19% at short range to 65% at long range) and has been reported previously also for a wide range of organic dye molecules [38]. The CAM–B3LYP wavelengths are 26 nm, 33 nm and 40 nm smaller than the corresponding PBE0 values for molecules cis–**I**, cis–**II** and cis–**III**, respectively, and 37 nm, 45 nm and 53 nm smaller than the B3LYP results. It can be seen that the above-mentioned differences between functionals increase with the growing donor–acceptor strength of substituents. In other words, the larger the reorganisation of electron density upon photoexcitation for the system, the larger its sensitivity to the amount of exact exchange in the functional. It is worth noting that, for a typical push–pull molecule such as 4-nitroaniline, the corresponding difference between B3LYP and CAM–B3LYP λ_{max} is of the order of 20 nm [22]. Moreover, results obtained by Jacquemin et al. [38] for a series of substituted azobenzene molecules reveal an analogous behaviour of wavelength values with the increasing charge–transfer character calculated for various functionals.

It has been shown previously that even the tiny change in geometry of the investigated system can create large shifts in the position of the calculated UV–VIS bands [11]. Particularly important for the correct prediction of the excitation energy in azobenzene derivatives is the N=N bond length. To further investigate the reason for the surprisingly good B3LYP performance in wavelength prediction in comparison to the new generation CAM–B3LYP functional, geometry optimisation of cis–**I** was carried out in the gas phase at the MP2/6–311++G(d,p) level of theory. The obtained differences with respect to the B3LYP/6–311++G(d,p) structure are small, with a change in N=N distance of 0.03 Å, but, as presented in Table 1, this causes a shift in the corresponding DFT wavelengths of the order of 10 nm in the case of the more interesting $\pi \rightarrow \pi^*$ transition. The influence of the optimised geometry was additionally investigated at the RI–CC2 level of theory. The calculated spectra for B3LYP/6–311++G(d,p) and MP2/6–311++G(d,p) optimised geometries gave signals corresponding to the $1^1A \rightarrow 3^1A$ transition at 273 nm and 274 nm, respectively. This shows clearly that RI–CC2 spectra are not as sensitive to geometry differences as DFT data for the employed basis set. One should also note that these values are close to the CAM–B3LYP results, and significantly underestimate the corresponding wavelength.

Figure 2 presents the experimental spectra recorded in 1,1,2–trichloroethane for the photostationary state obtained by irradiation of a sample containing trans-isomers of the investigated molecules. The maxima for absorption bands are located at 308 nm and 441 nm for **I**, at 367 nm and 415 nm for **II**, and at 271 nm, 383 nm and 450 nm for **III**. Since the sample in each case corresponds to the photostationary state, in addition to the cis-isomer, the trans-form is also present in solution. Therefore, one can distinguish bands in the spectra arising from both isomeric forms. On the basis of earlier data [1] and present results (summarised in Table 2), the signals appearing at 415 nm for **II** and 450 nm for **III** can be ascribed to trans-conformers. The low-intensity $n \rightarrow \pi^*$ transition bands are overlapped by $\pi \rightarrow \pi^*$ transitions signals of much larger intensity.

The wavelengths and oscillator strengths calculated with inclusion of solvent effects are presented in Table 1. Due to computational limitations, only the values of B3LYP and PBE0 excitation energies are given. The theoretical values

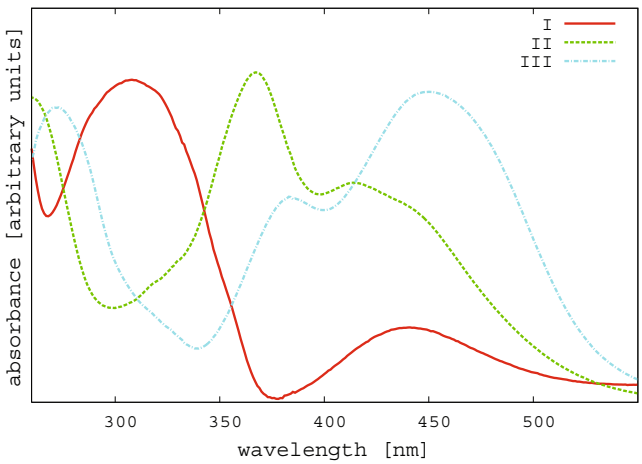

Fig. 2 Experimental UV–VIS spectra of investigated molecules in 1,1,2–trichloroethane

Table 2 Excitation energies (ΔE) and oscillator strengths (f) calculated at the TDDFT/6–311++G(d,p) level of theory with the inclusion of the solvent effects by the integral equation formalism for the polarisable continuum (IEF-PCM) model

	B3LYP		PBE0	
	λ_{max}	f	λ_{max}	f
I				
2^1A	472	0.06	463	0.05
3^1A	313	0.07	301	0.10
4^1A	305	0.06	295	0.06
II				
2^1A	491	0.12	482	0.11
3^1A	361	0.34	350	0.37
4^1A	310	0.03	299	0.04
III				
2^1A	498	0.17	489	0.16
3^1A	383	0.30	370	0.35
4^1A	316	0.13	304	0.09

of B3LYP excitation energies agree very well with the location of the experimental maxima of the $\pi \rightarrow \pi^*$ transition; the difference does not exceed 5 and 6 nm for cis–**I** and cis–**II**, respectively. In the case of cis–**III**, the experimental and theoretical values are identical.

Small solvatochromic shifts can be expected for the investigated systems in a solvent with a relatively small dielectric constant such as 1,1,2–trichloroethane. The incorporation of solvent effects for the 3^1A excited state brings about a redshift of the calculated absorption bands from 7 nm (PBEO for cis–**I**) to 14 nm (B3LYP and PBEO values for cis–**III**). Indeed, it has been shown previously that, for azobenzene derivatives, enhancement of medium polarity induces only minor solvent shifts in the UV–VIS spectrum [12, 13]. In order to answer the question of whether the solvent affects mostly the geometry of the investigated system, thereby causing a shift in the spectral bands, or influences mainly the spectrum itself, calculations of the spectra in vacuo and with inclusion of environmental effects were performed on both vacuum and solvent-optimised structures of cis–**I**. In comparison to the gas phase spectrum for gas phase geometry ($1^1A \rightarrow 3^1A$ transition at 305 nm), the signal shift is negligible for the 1,1,2–trichloroethane spectrum calculated for vacuum geometry ($1^1A \rightarrow 3^1A$ transition at 306 nm); however, the shift is significant for 1,1,2–trichloroethane spectrum at solvent-optimised geometry ($1^1A \rightarrow 3^1A$ transition at 313 nm). The shift occurring here is of the same order of magnitude as the shift observed in vacuo at the B3LYP level for geometries obtained by means of various methods (see Tables 1, 2). This confirms that an accurate geometry seems to be crucial for adequate determination of the UV–VIS spectra at the DFT level of theory. Moreover, one can distinguish between the $n \rightarrow \pi^*$ transition undergoing a blue-shift and $\pi \rightarrow \pi^*$ transitions subjected to a red-shift upon the inclusion of solvent effects. It should be stressed, however, that the intrinsic character of the transitions is more complicated than the conventionally used $n \rightarrow \pi^*$ and $\pi \rightarrow \pi^*$ classification. Analysis of the molecular orbital coefficients indicates clearly that those transitions have a mixed character.

Two-photon absorption spectra

In addition to the linear spectral calculations presented and discussed above, two-photon absorption spectra are also of interest. In this contribution, we report on values of two-photon absorption probability determined in isotropic medium with both photons of the same energy, polarised linearly and with parallel orientation [40]:

$$\left\langle \delta^{0F} \right\rangle = \frac{1}{15} \sum_{ij} \left[S_{ii}^{0F} \left(S_{jj}^{0F} \right)^* + 2 S_{ij}^{0F} \left(S_{ij}^{0F} \right)^* \right], \tag{1}$$

where S_{ij}^{0F} is the second-order transition moment defined as:

$$S_{ij}^{0F}(\zeta_1, \zeta_2) = \frac{1}{\hbar} \sum_K \left[\frac{\langle 0|\zeta_1 \cdot \hat{\mu}_i|K\rangle \left\langle K|\zeta_2 \cdot \hat{\mu}_j|F\right\rangle}{\omega_K - \omega_1} + \frac{\langle 0|\zeta_2 \cdot \hat{\mu}_i|K\rangle \left\langle K|\zeta_1 \cdot \hat{\mu}_j|F\right\rangle}{\omega_K - \omega_2} \right]. \tag{2}$$

The sum of photon energies $\hbar\omega_1 + \hbar\omega_2$ should satisfy the resonance condition with the final state F, and $\langle K|\zeta_1 \cdot \hat{\mu}|L\rangle$ is the transition moment between electronic states K and L, respectively. Since, in most experiments, one source of photons is used, one can substitute $0.5 \cdot \omega_F$ for the angular frequencies ω_1 and ω_2. The results of calculations of $\langle \delta \rangle$ using different DFT functionals and HF wavefunction for the low-lying 3^1A excited electronic state are presented in Table 3. It is now well established that conventional functionals suffer from an "overshooting" problem for nonlinear optical properties [41–43]. Hence, it is not surprising that one observes very large discrepancies between the B3LYP (or PBEO) and the CAM–B3LYP values of $\langle \delta \rangle$. The HF results are the lowest estimate of $\langle \delta \rangle$ due to the lack of electron correlation effects. Despite the differences in the values at different levels of theory, the data presented in Table 3 are sufficient to draw the following conclusion: as the strength of the donor–acceptor substituents increases, one observes substantial enhancement of the two–photon absorption probability, i.e. the values of $\langle \delta \rangle$ for **III** are an order of magnitude larger than those calculated for **I**.

A comparison of the calculated two-photon absorption cross-section with experimental data may be achieved based on the following relation:

$$\sigma_{0F}^{(2)} = \frac{8\pi^3 \alpha^2 \hbar^3}{e^4} \frac{\omega^2 g(\omega)}{\Gamma_F/2} \langle \delta \rangle, \tag{3}$$

Table 3 Values (in atomic units) of two-photon transition probability to the 3^1A electronic excited state calculated for isolated systems using 6–31+G(d) basis set

	cis-**I**	cis-**II**	cis-**III**	trans-**I**	trans-**II**	trans-**III**
HF	95 (235 nm)	2,090 (255 nm)	2,930 (264 nm)	2 (286 nm)	130 (285 nm)	6,310 (317 nm)
PBE0	1,370 (293 nm)	9,130 (337 nm)	13,300 (356 nm)	218 (332 nm)	11,800 (366 nm)	24,500 (401 nm)
B3LYP	1,460 (304 nm)	9,440 (348 nm)	13,800 (365 nm)	296 (343 nm)	14,200 (384 nm)	24,800 (415 nm)
CAM–B3LYP	533 (268 nm)	7,600 (303 nm)	10,600 (315 nm)	37 (314 nm)	2,660 (323 nm)	18,300 (368 nm)

where α is the fine structure constant, $\hbar\omega$ is the energy of absorbed photons (assuming a single source of photons), Γ_F is the lifetime broadening of the final state and $g(\omega)$ is the spectral line profile, which is assumed here to be the δ–function.

Unfortunately, we aware of no experimental data concerning two-photon absorption spectra for the systems investigated here. However, Antonov et al. reported $\sigma^{(2)}$ values for a compound similar to **III**, i.e. an azobenzene molecule substituted with cyano and dimethylamino groups (denoted as **aN=ND**) [45, 46]. The experimentally determined $\sigma^{(2)}$ value in DMSO was found to be 77 GM. Values of 50 GM and 110 GM were reported by De Boni et al. [44] for Disperse Orange 3 (DO3) and Disperse Red 1 (DR1), respectively, likewise with measurements performed in DMSO. The large increase in $\sigma^{(2)}$ value on going from the DO3 to the DR1 molecule is due solely to the substituent. For the purpose of critical assessment of the functionals employed here, we performed additional calculations of $\sigma^{(2)}$ for the **aN=ND** molecule studied experimentally by Antonov et al. [45]. Table 4 presents the values of $\sigma^{(2)}$ for **aN=ND** calculated according to Eq. 3, with the value of Γ_F equal to 2,020 cm^{-1} [45]. We used both the theoretical excitation energy (see Eq. 3) for the isolated molecule and the experimental value measured in DMSO. It is interesting to note that our values of $\sigma^{(2)}$ are much larger than those reported by Antonov et al. [45, 46] and even than those presented by De Boni et al. [44] for DR1. The use of experimental excitation energy for evaluation of $\sigma^{(2)}$ brings a significant improvement, i.e. the CAM–B3LYP value decreases from 237 to 189 GM. We note, however, that the values of $\sigma^{(2)}$ evaluated using PBEO and B3LYP functionals are much larger than those calculated using CAM–B3LYP. Finally, we would like to point out the surprisingly good performance of HF wavefunction in calculations of $\sigma^{(2)}$ for the studied compound.

Table 4 Values (in GM) of two-photon absorption cross-section for **aN=ND** (see reference [45]) calculated using Eq. 3. The value of Γ_F was taken from [45]. Gas-phase excitation energy determined theoretically and experimental excitation energy measured in DMSO were employed for evaluation of $\sigma^{(2)}_{gas}$ and $\sigma^{(2)}_{DMSO}$, respectively

	HF	PBE0	B3LYP	CAM–B3LYP
$\langle\delta\rangle_{gas}$	5,550	18,600	18,700	14,900
$\sigma^{(2)}_{gas}$	147	312	295	295
$\sigma^{(2)}_{DMSO}$	70	236	237	189

Excited state dipole moments

The characteristic feature of donor–acceptor molecules is the existence of electronic excited states of significantly different polarity than the ground state, which can be observed experimentally with the aid of UV–VIS spectroscopy [48, 49]. The excitations to these states are usually of large intensity (i.e. of large oscillator strength value). The extent to which reorganisation of electronic density can take place is determined by the strength of donor and acceptor substituents and the character of the linkage between them. This can be described quantitatively by the dipole moment difference between the ground and excited state ($\Delta\mu$), and the transition intensity between the ground and excited state of interest. Although the transition intensity can be determined experimentally, $\Delta\mu$ cannot really be estimated with satisfactory accuracy from the experimental data. However, the value of $\Delta\mu$ can be calculated using ab initio methods with sufficient accuracy. It can be achieved both analytically (e.g. as the residue of a quadratic response function or from electron densities in excited states), or numerically (by differentiation of excitation energies with respect to the applied electric field). As mentioned in Computational methodology, the latter approach is adopted in the present study.

The dipole moments for the ground (1^1A) and excited (3^1A) state for the cis-azobenzene derivatives calculated within TDDFT formalism for all three investigated systems are presented in Table 5. The corresponding analysis for trans-conformers was presented in [1]. Functionals B3LYP and PBEO both provide similar results of dipole moment in the ground and the excited state. The maximal difference between PBEO and B3LYP values of μ does not exceed 1 D. The ground state dipole moment increases as the strength of the donor–acceptor substituents increases, i.e. the smallest μ value of the ground state is observed for molecule cis–**I** and

Table 5 Values (in [D]) of dipole moments for two singlet states, namely 1^1A and 3^1A calculated at the TDDFT/6–311++G(d,p) level of theory

	Gas phase		1,1,2–Trichloroethane	
	B3LYP	PBE0	B3LYP	PBE0
I				
1^1A	4.3	4.3	5.5	5.5
3^1A	5.0	4.8	9.1	8.2
II				
$_1^1A$	6.2	6.2	7.8	7.7
3^1A	12.1	12.2	13.9	14.1
III				
1^1A	8.2	8.2	10.3	10.2
3^1A	15.0	15.5	18.3	18.2

the largest for molecule cis–**III**. The inclusion of solvent effects leads to values of ground state dipole moments that are larger by 1.2–2.1 D in all cases analysed.

The gas-phase change in the dipole moment values occurring during the experimentally observed strong $\pi \rightarrow \pi^*$ transition are of the order of 1 D, 6 D and 7 D for cis–**I**, cis–**II** and cis–**III**, respectively. This is clear evidence of the increasing charge-transfer character of the transitions of interest in the sequence of molecules considered here. Corresponding values for solutions amount to about 3 D, 6 D and 8D for the given series of systems. The inclusion of solvent effects has a moderate influence on $\Delta\mu$ of cis–**II** and cis–**III**, but leads to significant changes in the $\Delta\mu$ value for cis–**I**: the dipole moment values for both 1^1A and 3^1A states of molecule cis–**I** are similar in the gas phase, but

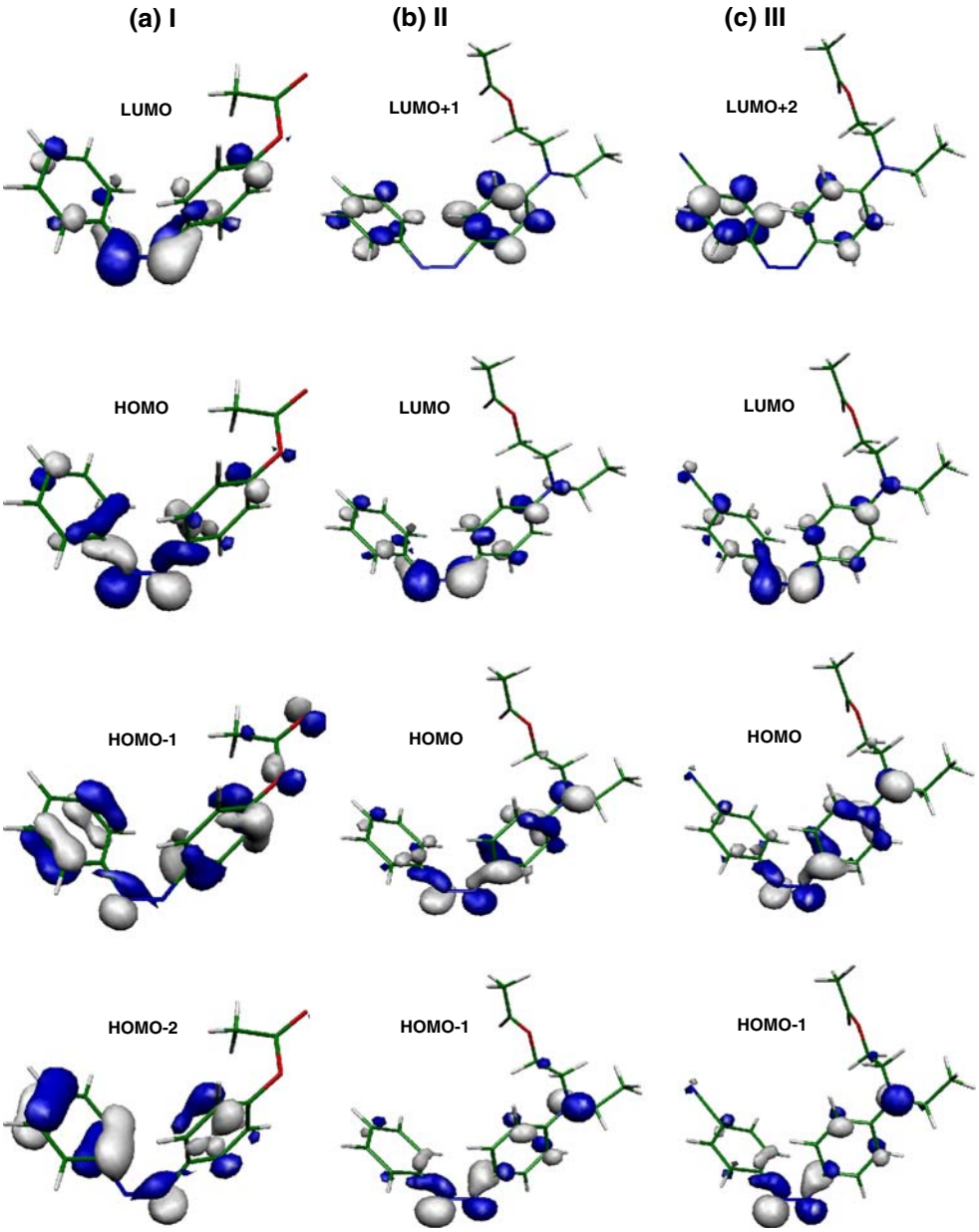

Fig. 3 Molecular orbitals involved in the investigated transitions, generated at B3LYP/6–311++G(d,p) level of theory for **a** cis–**I**, **b** cis–**II** and **c** cis–**III**

Table 6 Linear and non–linear electro-optical properties calculated using a finite-field approach based on B3LYP/6–311++G(d,p) geometries. All values are in atomic units

	μ_z	α_{xx}	α_{yy}	α_{zz}	β_{yyy}	β_{xxx}	β_{zzz}
cis–**I**							
BLYP/6–31+G(d)	−4.43	182.4	259.1	669.4	−50.1	−27.0	−14,772.1
LC–BLYP/6–31+G(d)	−3.83	173.9	244.0	522.4	−43.8	40.4	−9,901.3
HF/6–31+G(d)	−3.83	165.3	229.2	470.7	−44.3	83.6	−6,915.4
MP2/6–31+G(d)	−3.64	173.6	241.0	519.2	−67.4	−36.1	−13,765.1
cis–**II**							
BLYP/6–31+G(d)	−2.54	205.4	298.6	322.3	−27.4	−178.2	−3,197.0
LC–BLYP/6–31+G(d)	−2.32	197.1	271.3	280.7	−21.7	−74.9	−1,997.7
HF/6–31+G(d)	−2.29	187.6	254.5	254.3	−26.8	−7.91	−1,271.9
MP2/6–31+G(d)	−2.31	196.4	266.2	279.5	−21.8	−119.9	−2,364.5
cis–**II**							
BLYP/6–31+G(d)	−3.43	214.6	310.8	389.6	13.0	9.73	−4,591.3
LC–BLYP/6–31+G(d)	−2.99	205.9	284.2	330.1	−5.6	20.8	−2,769.8
HF/6–31+G(d)	−2.89	196.4	260.5	302.8	24.2	−2.6	−1,716.6
MP2/6–31+G(d)	−2.87	204.8	280.9	324.4	9.4	88.3	−3,453.4
trans–**I**							
BLYP/6–31+G(d)	1.82	163.2	174.2	361.1	−235.7	−9.8	−1,701.9
LC–BLYP/6–31+G(d)	1.96	147.1	168.3	300.7	−36.2	−5.8	−452.7
HF/6–31+G(d)	2.07	138.8	162.5	279.4	−39.2	−4.5	−321.8
MP2/6–31+G(d)	1.88	145.1	166.1	291.9	−40.1	−6.8	−371.6
trans–**II**							
BLYP/6–31+G(d)	−0.82	340.2	352.2	233.9	−2,994.9	−2,164.6	197.1
LC–BLYP/6–31+G(d)	−0.93	283.3	299.7	219.9	−727.5	−508.4	77.5
HF/6–31+G(d)	−0.99	264.6	278.3	207.3	−428.6	−320.1	65.5
MP2/6–31+G(d)	−0.86	277.4	291.8	218.7	−685.0	−483.5	218.7
trans–**III**							
BLYP/6–31+G(d)	−4.43	182.4	259.1	669.4	−50.1	−27.0	−14,772.1
LC–BLYP/6–31+G(d)	−3.83	173.9	244.0	522.4	−43.8	40.4	−9,901.3
HF/6–31+G(d)	−3.83	165.3	229.2	470.7	−44.3	83.6	−6,915.4
MP2/6–31+G(d)	−3.64	173.6	241.0	519.2	−67.4	−36.1	−13,765.1

in 1,1,2–trichloroethane the second singlet excited state becomes considerably more polar than the ground state.

Figure 3 presents the molecular orbitals involved in the transitions discussed in this contribution calculated for the gas phase at the B3LYP/6–311++G(d,p) level of theory. The HOMO-1–LUMO transition corresponds to the most intensive band in the spectrum. For cis–**II** and cis–**III**, a considerable asymmetric reorganisation of charge occurs from the amino group to the double N=N bond region, which corresponds to a significant change in the dipole moment when passing from the ground state to the excited 3^1A state. However, for cis–**I**, the shift in the charge distribution lacks such obvious asymmetry, therefore the observed dipole moment difference between ground and excited states is much smaller than in the case of the other systems.

Nonlinear optical properties

In this section, we shall present and discuss the results of calculations of electric properties without taking environmental effects into account. In particular, we will focus on first-order hyperpolarisability (β), which is defined as one of the coefficients appearing in the Taylor expansion of the energy of a system with respect to the static electric field:

$$E(F) = E(0) - \mu_i F_i - \frac{1}{2!}\alpha_{ij}F_iF_j - \frac{1}{3!}\beta_{ijk}F_iF_jF_k - \frac{1}{4!}\gamma_{ijkl}F_iF_jF_kF_l - \ldots, \quad (4)$$

Table 7 First–order hyperpolarisability of the investigated systems calculated at the MP2/6–31+G(d)//B3LYP/6–311++G(d,p) level of theory

	cis-**I**	cis-**II**	cis-**III**	trans-**I**	trans-**II**	trans-**III**
$\beta[au]$	−140	1,648	2,600	−279	−486	16,691
$\beta \cdot 10^{-3}[esu]$	−1	14	22	−2	−4	144

where $E(0)$ is the field free energy of a molecular system. In the present study, the tensor components of α and β were evaluated by numerical differentiation of the total energy with respect to the field strength F [34]. As mentioned above, traditional functionals tend to overshoot the values of molecular (hyper)polarisabilities [41–43]. It seems, however, that successful prediction of α, β and γ by LRC functionals depends greatly on the investigated system [47]. Thus, it was of great interest to investigate the performance of the recently developed LC–BLYP functional in calculations of β in the studied systems. The values of β computed at the MP2/6–31+G(d) level of theory shall serve here as a reference. Table 6 presents the results of calculations of diagonal components of the first-order hyperpolarisability together with the values of α and μ. The molecules were oriented in such a way as to make the dipole moment vector [calculated at the B3LYP/6–311++G(d,p) level of theory] parallel to the Cartesian z axis. With the exception of trans–**II**, we see that the diagonal component of β along the dipole moment vector is dominant. It is clearly seen that the values of β_{zzz} calculated using the BLYP functional are significantly larger than the corresponding values calculated at the MP2 level of theory. This is consistent with results presented by Masunov et al. for a series of donor–acceptor π-conjugated systems [35]. However, the LC–BLYP functional improves substantially upon BLYP for the diagonal β_{zzz} component. In most cases, the absolute values of first-order hyperpolarisability calculated using the LC–BLYP functional are smaller than those calculated at the MP2 level of theory. The analogous trend is observed also for α. Similar to results for $\sigma^{(2)}$, the HF results constitute the lowest estimate of molecular (hyper)polarisabilities.

It is noteworthy that the electron correlation effects are quite substantial, i.e. −1,717 a.u. vs −3,453 a.u., and −6,915 a.u. vs −13,765 a.u. for the cis- and trans-isomers of **III**, respectively. In order to relate the properties to the structure of investigated systems, the rotationally invariant first-order hyperpolarisability was calculated according to the following expression:

$$\overline{\beta} = \sum_{i=x,y,z} \frac{\mu_i \beta_i}{|\mu|}, \tag{5}$$

where

$$\beta_i = \frac{1}{5} \sum_{j=x,y,z} \left(\beta_{ijj} + \beta_{jij} + \beta_{jji}\right). \tag{6}$$

The results of computations (presented in Table 7) are consistent with what has been observed for two-photon absorption probabilities, i.e. β increases substantially on going from **I** to **III**.

Conclusions

The spectroscopic parameters of three cis-azobenzene derivatives were analysed by means of the TDDFT method to complement our previously published data [1]. The results obtained clearly show that the most important factors in the calculation setup are the proper geometry and an adequate functional choice for the UV–VIS spectra simulation. Even minor N=N bond length variation can strongly affect the position of the bands in the DFT spectrum. However, for the most common choice of methodology—the B3LYP functional—exceptional agreement of computed and experimental data is observed. At the B3LYP/6–311++G(d,p) geometry, B3LYP seems to significantly outperform the range-separated CAM–B3LYP and LC–BLYP functionals in the calculated wavelengths.

Nonlinear optical properties, namely two-photon absorption cross-sections and first-order hyperpolarisabilities, were also calculated for both cis- and trans-isomers. Contrary to conclusions drawn based on the performance of the functionals employed in calculations of UV–VIS spectra, the CAM–B3LYP functional gives values for two-photon absorption cross-sections that are much closer to experimental data, outperforming traditional B3LYP and PBEO functionals. It is noteworthy that the values of first-order hyperpolarisabilities closely follow the trend observed for two-photon absorption cross-sections as the strength of the donor–acceptor character of the azobenzene derivatives increases.

Acknowledgements The authors gratefully acknowledge the allotment of CPU time at the Poznan Supercomputing and Networking Centre (PCSS), ACK Cyfronet and Wroclaw Center of Networking and Supercomputing (WCSS). The work was (partly) supported by the European Commission through the Human Potential Programme (Marie-Curie RTN BIMORE, GRANT No. MRTN-CT-2006-035859).

References

1. Zaleśny R, Matczyszyn K, Kaczmarek A, Bartkowiak W, Cysewski P (2007) J Mol Model 13:785
2. Granucci G, Persico M (2007) Theor Chem Acc 117:1131
3. Cembran A, Bernardi F, Garavelli M, Gagliardi L, Orlandi G (2004) J Am Chem Soc 126:3234
4. Cattaneo P, Persico M (1999) Phys Chem Chem Phys 1:4739
5. Ishikawa T, Noro T, Shoda T (2001) J Chem Phys 115:7503
6. Boeckmann M, Doltsinis N, Marx D, Phys Rev Lett, submitted
7. Crecca CR, Roitberg AE (2006) J Phys Chem A 110:8188
8. Kawata S, Kawata Y (2000) Chem Rev 100:1777
9. Ikeda T, Tsutsumi O (1995) Science 268:1873
10. Liu ZF, Hashimoto K, Fujishima K (1990) Nature 347:658
11. Hättig C, Hald K (2002) Phys Chem Chem Phys 4:2111
12. Grasso D, Millefiori S, Fasone S (1975) Spectrochim Acta A 31:187
13. Pedersen TG, Ramanujam PS, Johansen PM, Hvilsted S (1998) J Opt Soc Am B 15:2721
14. Foresman JB, Head-Gordon M, Pople JA, Frisch MJ (1992) J Phys Chem 96:135
15. Burke K, Werschnik J, Gross EKU (2005) J Chem Phys 123:062206
16. Marques MAL, Gross EKU (2004) Annu Rev Phys Chem 55:427

17. Appel H, Gross EKU, Burke K (2003) Phys Rev Lett 90:043005
18. Furche F, Ahlrichs R (2002) J Chem Phys 117:7433
19. Sałek P, Vahtras O, Helgaker T, Ågren H (2002) J Chem Phys 117:9630
20. Jansik B, Sałek P, Jonsson D, Vahtras O, Ågren H (2005) J Chem Phys 122:054107
21. Miura M, Aoki Y, Champagne B (2007) J Chem Phys 127:084103
22. Rudberg E, Sałek P, Helgaker T, Ågren H (2005) J Chem Phys 123:184108
23. Yanai T, Tew DP, Handy NH (2004) Chem Phys Lett 393:51
24. Peach MJG, Helgaker T, Sałek P, Keal TW, Lutnaes OB, Tozer DJ, Handy NC (2006) Phys Chem Chem Phys 8:558
25. Jacquemin D, Perpéte EA, Scalmani G, Frisch MJ, Kobayashi R, Adamo C (2007) J Chem Phys 126:144105
26. Hättig C, Weigend F (2000) J Chem Phys 113:5154
27. Ahlrichs R, Bär M, Häser M, Horn H, Kölmel C (1989) Chem Phys Lett 162:165
28. Hättig C (2005) Phys Chem Chem Phys 7:59
29. Gaussian O3, Revision C.O2, Frisch MJ, Trucks GW, Schlegel HB, Scuseria GE, Robb MA, Cheeseman JR, Montgomery Jr JA, Vreven T, Kudin KN, Burant JC, Millam JM, Iyengar SS, Tomasi J, Barone V, Mennucci B, Cossi M, Scalmani G, Rega N, Petersson GA, Nakatsuji H, Hada M, Ehara M, Toyota K, Fukuda R, Hasegawa J, Ishida M, Nakajima T, Honda Y, Kitao O, Nakai H, Klene M, Li X, Knox JE, Hratchian HP, Cross JB, Bakken V, Adamo C, Jaramillo J, Gomperts R, Stratmann RE, Yazyev O, Austin AJ, Cammi R, Pomelli C, Ochterski JW, Ayala PY, Morokuma K, Voth GA, Salvador P, Dannenberg JJ, Zakrzewski VG, Dapprich S, Daniels AD, Strain MC, Farkas O, Malick DK, Rabuck AD, Raghavachari K, Foresman JB, Ortiz JV, Cui Q, Baboul AG, Clifford S, Cioslowski J, Stefanov BB, Liu G, Liashenko A, Piskorz P, Komaromi I, Martin RL, Fox DJ, Keith T, Al-Laham MA, Peng CY, Nanayakkara A, Challacombe M, Gill PMW, Johnson B, Chen W, Wong MW, Gonzalez C, Pople JA, Gaussian, Inc., Wallingford CT (2004)
30. Cancés MT, Mennucci B, Tomasi J (1997) J Chem Phys 107:3032
31. DALTON, a molecular electronic structure program, Release 2.0 (2005), see http://www.kjemi.uio.no/software/dalton/dalton.html
32. Iikura H, Tsuneda T, Yanai T, Hirao K (2001) J Chem Phys 115:3540
33. Kamiya M, Sekino H, Tsuneda T, Hirao K (2005) J Chem Phys 122:234111
34. Kurtz HA, Stewart JJP, Dieter KM (1990) J Comp Chem 11:82
35. Suponitsky KY, Tafur S, Masunov AE (2008) J Chem Phys 129:044109
36. Jacquemin D, Bouhy M, Perpéte EA (2006) J Chem Phys 124:204321
37. Jacquemin D, Preat J, Wathelet V, Fontaine M, Perpéte EA (2005) J Am Chem Soc 128:2072
38. Jacquemin D, Perpéte EA, Scuseria G, Ciofini I, Adamo C (2008) J Chem Theory Comput 4:123
39. Perpéte EA, Wahtelet V, Preat J, Lambert C, Jacquemin D (2006) J Chem Theory Comput 2:434
40. Monson PR, McClain WM (1970) J Chem Phys 53:29
41. Champagne B, Perpète EA, van Gisbergen SJA, Baerends EJ, Snijders JG, Soubra-Ghaoui C, Robins KA, Kirtman B (1998) J Chem Phys 109:10489
42. Champagne B, Perpète EA, Jacquemin D, van Gisbergen SJA, Baerends EJ, Soubra-Ghaoui C, Robins KA, Kirtman B (2000) J Phys Chem A 104:4755
43. van Gisbergen SJA, Schipper PRT, Gritsenko OV, Baerends EJ, Snijders JG, Champagne B, Kirtman B (1999) Phys Rev Lett 83:694
44. De Boni L, Misoguti L, Zilio SC, Mendonça C (2005) ChemPhysChem 6:1121
45. Antonov L, Kamada K, Ohta K, Kamounah FS (2003) Phys Chem Chem Phys 5:1193
46. Ohta K, Antonov L, Yamada S, Kamada K (2007) J Chem Phys 127:084504
47. Kirtman B, Bonness S, Ramirez-Solis A, Champagne B, Matsumoto H, Sekino H (2008) J Chem Phys 128:114108
48. Reichardt C (1994) Chem Rev 94:2319
49. Bartkowiak W (2006) Solvatochromism and nonlinear optical properties of donor–acceptor π-conjugated molecules. In: Papadopoulos MG, Sadlej AJ, Leszczynski J (eds) Non-linear optical properties of matter. Springer, Berlin